Available online at www.sciencedirect.com

SciVerse ScienceDirect

Ceramics International 39 (2013) 6433–6440

CERAMICS INTERNATIONAL

www.elsevier.com/locate/ceramint

Electrical properties of Tb-doped barium cerate

Q.A. Islam, S. Nag, R.N. Basu*

Fuel Cell and Battery Division, CSIR-Central Glass and Ceramic Research Institute, 196 Raja S.C. Mullick Road, Kolkata 700032, India

Received 13 October 2012; received in revised form 27 December 2012; accepted 22 January 2013
Available online 6 February 2013

Abstract

The electrical conductivity of $Ba_{0.8}Ce_{1-x}Tb_xO_{3-\delta}$ ($0 \le x \le 0.15$) has been studied in air and moist reducing atmosphere (5% H_2 in Ar) in the temperature range between 550 and 900 °C. The powders of such materials are prepared by the combustion synthesis technique. The microstructure of the sintered specimens correlates well with its electrical properties. Electrical conduction mechanism of sintered specimens in various atmospheres is explained with respect to defect sites formed within the material. The generation of hydroxyl vacancy, proton and hole in moist reducing atmosphere increases the protonic conductivity significantly compared to hole/oxide ion conductivity in air atmosphere. Grain and grain boundary conductivity have been determined from the impedance measurements. The complex mechanism of electrical conduction of the sintered materials does not follow the linear behaviour in the Arrhenious plot. Maximum electrical conductivity obtained under moist reducing atmosphere is 0.049 S cm^{-1} for $Ba_{0.8}Ce_{0.85}Tb_{0.15}O_{3-\delta}$ at 900 °C.

Keywords: B. X-ray methods; B. Defects; C. Electrical Properties; C. Impedance; Microstructure

1. Introduction

The rare earth doped barium cerate perovskite materials are being investigated over the decades for variety of applications such as gas separation membrane, gas sensor, electrolyte for solid oxide fuel cell, catalyst and in nuclear power plant [1–11]. These oxides have both the oxide ion conductivity as well as proton conductivity depending upon the operating temperature, surrounding gas atmosphere etc. The oxide ion vacancies through which the oxide ion migrates are being created by substitution of higher valance cations in B^{4+} site with lower valance cations (M^{3+}) in ABO_3 perovskite structure Eq. (1). On the other hand, the conversion of oxide ion conductivity to protonic conductivity is primarily due to the hydration of oxide ion vacancies Eq. (2) [5,7,12]. These vacancies are only able to migrate inside the materials whereas the dopants remain fixed in the B site of the ABO_3 perovskite structure.

$$2B_B^X + M_2O_3 + O_O^X = 2M_B^{'} + V_O^{\bullet\bullet} + 2BO_2 \quad (1)$$

$$H_2O(g) + V_O^{\bullet\bullet} + O_O^X \leftrightarrow 2OH_O^{\bullet} \quad (2)$$

However, the factors responsible for electrical conduction in these materials are the surrounding gas atmosphere, operating temperature, concentration of defect sites as well as charged species in the lattice structure, thickness of the material, materials synthesis procedure and the electric potential applied across the material [1,8,13–15]. Therefore, the conduction mechanism for this type of oxide is very complex. Understanding of the mechanism of electrical conduction in different atmospheres and operating temperatures is very much essential to enhance the performance of the material. However, a concrete study on the conduction mechanism particularly for this Tb-doped perovskite material has not been done extensively. In this investigation an attempt has been made to explore the conduction mechanism of Tb-doped barium cerate [$Ba_{0.8}Ce_{1-x}Tb_xO_{3-\delta}$ ($0 \le x \le 0.15$)] in air and moist reducing atmosphere.

2. Experimental

Tb-doped barium cerate powder of compositions $Ba_{0.8}Ce_{1-x}Tb_xO_{3-\delta}$ ($x = 0.3$, 0.5 and 0.7) are prepared by the combustion synthesis technique using $Ba(NO_3)_2$ [99+%, ACROS Organics], $Ce(NO_3)_3 \cdot 6H_2O$ [99.5%, ACROS

*Corresponding author. Tel.: +91 33 24292951; fax: +91 33 2473 0957.
E-mail addresses: rajenbasu54@gmail.com, rnbasu@cgcri.res.in (R.N. Basu).

0272-8842/$ - see front matter © 2013 Elsevier Ltd and Techna Group S.r.l. All rights reserved.
http://dx.doi.org/10.1016/j.ceramint.2013.01.071

Organics], $Tb(NO_3)_3 \cdot 5H_2O$ [99.9%, Sigma Aldrich] and CH_2NH_2COOH [99+%, ACROS Organics] as primary constituents. The nitrates of Ba, Ce and Tb are used as oxidants and glycine is used as fuel in this synthesis. Table 1 shows the four different compositions along with their respective identification codes which are used in this study. Barium deficient pure barium cerate is not stable at higher temperature but with addition of dopants the stability increases for such barium deficient compositions. In this study, the barium deficient composition is chosen because of its better chemical stability than stoichiometric or barium excess compositions [16,17]. All the combustion experiments have been performed in fuel rich condition (nitrate: fuel = 0.17). The thermal decomposition of gel precursor has been analyzed by DTA/TGA in air atmosphere at a heating rate of 10 °C/min using Simultaneous Thermal Analyzer (STA 409C, Netzsch, Germany). The as-synthesized powder is calcined at 1100 °C/6 h in air to form the phase-pure perovskite structure which is then confirmed by X-ray diffraction (XRD) analysis using X'Pert Pro software (PANalytical, Philips, Holland). The calcined powder is then planetary milled at a speed of 250 rpm for 6 h in isopropyl alcohol followed by air drying and pressing the powder uniaxially in the form of pellets (dia: 10 mm and thickness: 1–2 mm) under an applied pressure of 250 MPa followed by sintering at 1550 °C/6 h in air. The densities of the sintered specimens are measured by Archimedes principle using xylene as the immersion liquid. The compositional homogeneity across the sample equilibrated under air as well as moist reducing atmosphere at 900 °C is also confirmed by the SEM EDX (Leo S430i). The fractured surface morphology of the sintered samples has been observed by FESEM (Model no. SUPRA 35VP). The electrical conductivity is measured by complex plane AC impedance spectroscopy using a Frequency Response Analyser (ModuLab, Solartron, UK) in the frequency range of 10 μHz to 1 MHz. A symmetric cell configuration of Pt-barium cerate-Pt has been used for all the measurements. For this purpose, the electrodes are prepared by screen printing of pure platinum paste on the both sides of the sintered specimens followed by curing at 1000 °C/2 h in air. The electrical conductivity is measured in the temperature range between 550 and 900 °C in air as well as in moist reducing atmosphere (5% H_2 in Ar). The moist reducing atmosphere is created by passing the mixture gas (5% H_2 + 95% Ar) continuously through the water bubbler kept at room temperature during the electrical measurement. To obtain the environmental equilibrium the sintered pellet is kept for half an hour at each temperature before measurement in air as well as in moist reducing atmosphere.

Table 1
Sample identification codes of various Tb-doped $Ba_{0.8}CeO_{3-\delta'}$ compositions.

Tb doping (mol%)	Composition	Sample identification code
0	$Ba_{0.8}CeO_{3-\delta'}$	BC
5	$Ba_{0.8}Ce_{0.95}Tb_{0.05}O_{3-\delta''}$	BCT1
10	$Ba_{0.8}Ce_{0.90}Tb_{0.10}O_{3-\delta'''}$	BCT2
15	$Ba_{0.8}Ce_{0.85}Tb_{0.15}O_{3-\delta''''}$	BCT3

3. Results & discussion

The thermal analysis of the precursor gels of all four compositions shows that major weight loss is observed between 200 and 425 °C (Fig. 1). This broad temperature range indicates that the thermal decomposition in the precursor gel is gradual rather than instantaneous. During the combustion of the gel precursor, adsorbed and structural water is lost at the beginning up to around 200 °C. The weight loss in between 200 and 350 °C is due to the thermal decomposition of glycine complex and formation of respective oxide constituents. The formation of solid solution between the oxide constituents followed by phase evaluation corresponds to the weight loss in the temperature range 350–425 °C [18]. However, a minor amount of weight loss is still observed in all the compositions at around 900 °C which could be due to the formation of oxygen ion vacancy in the lattice structure [19]. It is reported that such oxygen ion vacancies are formed in undoped as well as doped barium cerate compositions which can be expressed by the Eqs. (3) and (4) [20,21]. The percentage of weight loss is found to be maximum in BC (94.03%) compared to doped compositions in the order of 84.12%, 84.71% and 83.27% for BCT1, BCT2 and BCT3 respectively (Table 1). It may be due to the presence of maximum percentage of structural water as well as glycine in the precursor gel of pristine composition (BC). By substitution of Ce with Tb, the structural water is reduced in the overall composition in the order of BCT1 > BCT2 > BCT3 because terbium nitrate contains five molecules of water compared to cerium nitrate which is hexahydrate. Therefore, the process of substitution of Ce by Tb actually reduces one molecule of water in overall composition. As the nitrate to glycine ratio is constant (0.17) for all the four compositions thus the amount of glycine is more in BC compared to doped compositions (BCT1, BCT2 and BCT3). It is also observed that there is no significant weight loss after 1100 °C which is

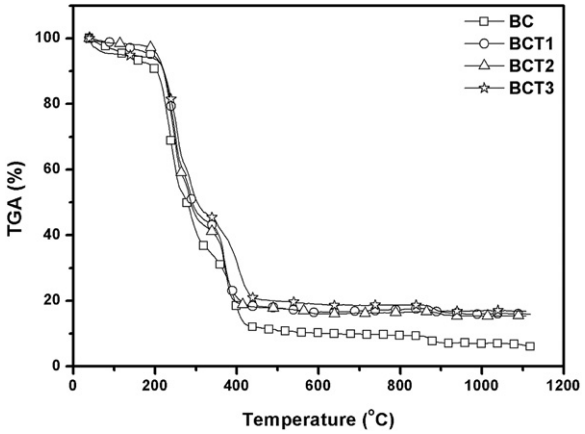

Fig. 1. TGA of $Ba_{0.8}CeO_{3-\delta'}$ and Tb-doped $Ba_{0.8}CeO_{3-\delta'}$.

indicative of minimum calcination temperature for the formation of perovskite phase.

The phase purity of the materials determined by X-ray powder diffraction analysis is shown in Fig. 2. The XRD shows that all the compositions are perovskite structure with a small presence of CeO_2. The corresponding 2θ positions for the CeO_2 phase are at 33.1°, 69.5° and 76.7° respectively. The segregation of this CeO_2 phase is due to the deficiency of Ba in Ba site [22]. The Ba deficient composition tries to stabilize itself in the stoichiometric ratio (Ba:Ce:O=1:1:3) and thus remove some CeO_2 from the composition which remains as free CeO_2 in the material. This segregating amount of CeO_2 is reduced with increasing Tb concentration as evident from the peak intensity of the CeO_2 phases. As the Tb concentration increases, the chances of segregating out of CeO_2 phase decrease. This is due to the formation of more stable phase with Tb doping [22]. The compositional homogeneity of the sintered specimens equilibrated for half an hour in air and moist reducing atmosphere at 900 °C is also shown in Table 2. The compositions thus obtained in both the atmospheres for surface and interior of the sample (BCT3) is almost similar. However, a small variation in data is well within the tolerance limit. The Rietveld analysis shows that the structures for all the four compositions are orthorhombic perovskite (space group pmcn). After doping Tb in barium cerate ($Ba_{0.8}Ce_{1-x}Tb_xO_{3-\delta}$) the majority of doped Tb ($r_{Tb^{3+}} = 1.18$ Å) should prefer the Ce ($r_{Ce^{4+}} = 1.11$ Å) sites and thereby create oxygen ion vacancies to conduct oxygen ions in moisture free dry oxygen atmosphere [23].

Fig. 3 shows the fractured surfaces of the undoped and doped barium cerate materials which appears to be the mixture of both intergranular and transgranular in nature. In undoped barium cerate (BC) the transgranular nature is more and with increasing Tb concentration transgranular nature is decreasing while intergranular nature is increasing. With increasing Tb concentration (BCT3 > BCT2 > BCT1), the materials are becoming more strained due to larger amount of Ce replaced by Tb [24]. Normally, when fracture occur the cracks has a tendency to propagate along the highly strained area rather than low strained area. Thus with increasing Tb doping, the defects, which are strained in nature, tries to segregate themselves along the grain boundary, therefore, the grain boundary area becomes more prone to crack propagation. Hence with increasing Tb concentration, the nature of fracture is gradually changing from transgranular to intergranular type. The average grain size is less in undoped barium cerate and is increased with Tb doping in BCT1. However, with further doping of Tb, the average grain size decreases in BCT2 and BCT3. The grain sizes as estimated from the microstructural studies are 1–2 μm in BC, 4–6 μm in BCT1, 2–4 μm in BCT2 and 3–4 μm in BCT3. Thus the average grain size is becoming smaller with increasing Tb concentration. The densities of the materials for all the four compositions are more than 99% of theoretical density when sintered in air at 1550 °C. The BET surface area of calcined powders for BC, BCT1, BCT2 and BCT3 are 11.4, 3.8, 6.0 and 13.2 m^2/g respectively. It clearly indicates that even though surface area values are varied between 3.8 and 13.2 m^2/g, all the materials showed extremely high density (almost close to that of theoretical values). The density of these materials needs to be high because during operation at elevated temperature it requires sufficient amount of ionic conduction [2,24]. The dense Tb-doped barium cerate material can be used as the ceramic part along with the metal (e.g. Ni, Pd etc.) to form mixed ionic and electronic conductor (MIEC) based cermet composite for gas separation membrane application. The presence of porosity in this material can lead to molecular transportation of the feed gas across the membrane, which in turn reduces the partial pressure difference between the feed and the permeate side and thereby reduces ionic conductivity. It is reported that the molecular transportation of the gas also reduces the purity of the permeate gas [25].

The electrical properties of these compositions have been determined using complex plane impedance analysis over a wide range of frequency (10 μHz–1 MHz). The electrical characterization of these materials has been done in air and moist reducing atmosphere in the temperature range from 550 to 900 °C. The electrical conductivity is the function of surrounding gas atmosphere, operating temperature, concentration of defect sites as well as charged species in the lattice

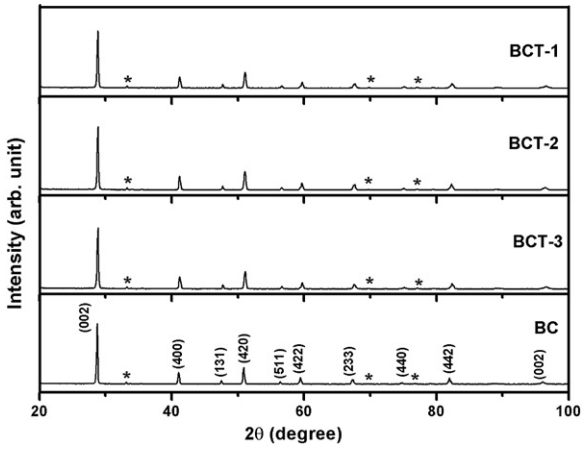

Fig. 2. X-ray diffraction patterns of $Ba_{0.8}CeO_{3-\delta}$ and Tb-doped $Ba_{0.8}CeO_{3-\delta}$ powders calcined at 1100 °C.

Table 2
Compositional homogeneity of BCT3 (surface and interior) equilibrated for 30 min at 900 °C in air and moist reducing atmosphere.

Sample	*Element*	**Element (%)**			
		Air		*Moist*	
		Surface	Interior	Surface	Interior
BCT3	Ba	38.75	35.74	38.27	35.80
	Ce	38.80	37.73	40.16	39.37
	Tb	5.42	6.07	6.00	5.86

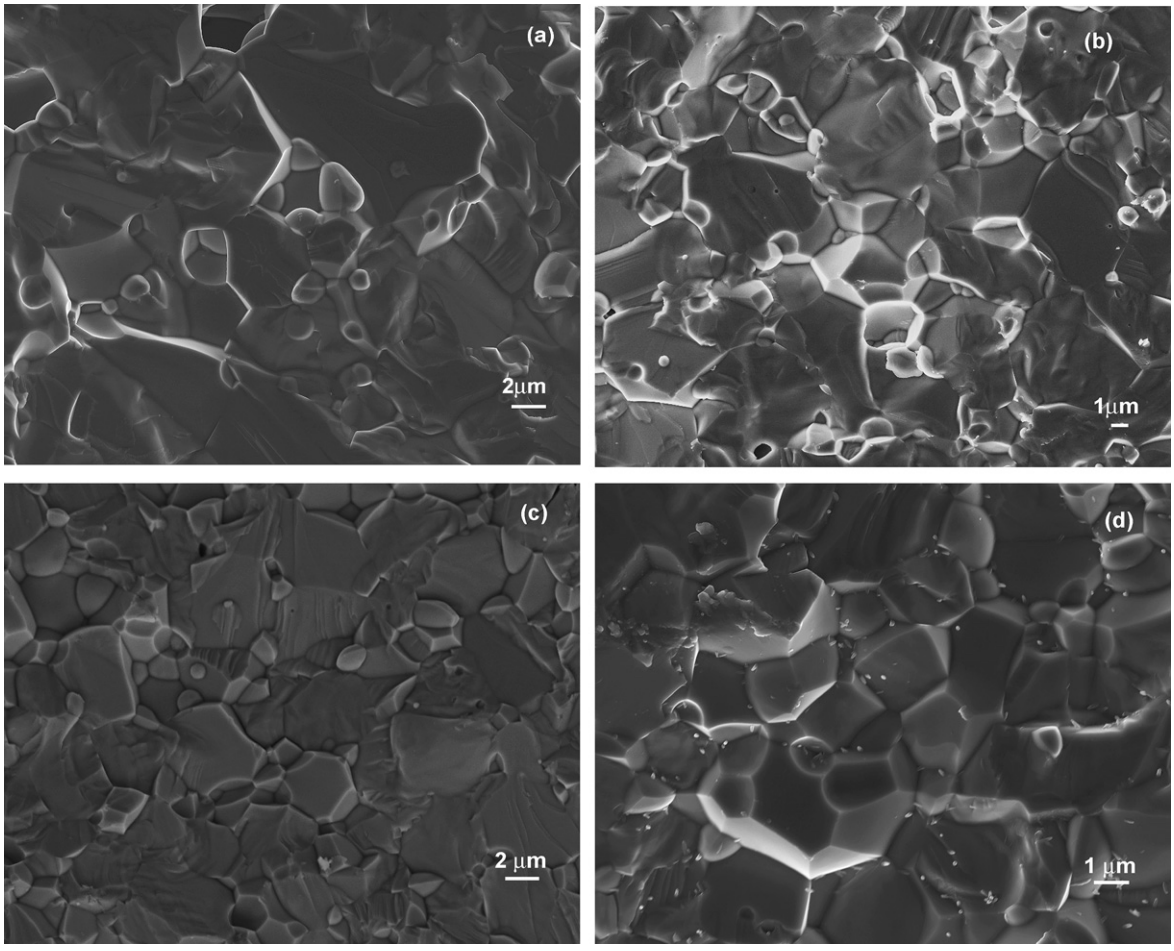

Fig. 3. Fractured surfaces of the specimen sintered at 1550 °C/6 h in air: (a) BC (b) BCT1 (c) BCT2 and (d) BCT3.

structure, thickness of the material and the electric potential applied across the material. The predomination of the charged species and defect sites in the lattice varies depending upon the operating temperature and surrounding atmosphere [26]. It has been observed that in air atmosphere the total conductivity (bulk and grain boundary) is increasing with increasing temperature for all the four compositions (Fig. 4a). In air atmosphere the defect sites in the lattice are oxygen ion vacancies and electron holes [27]. The oxygen ion vacancies are created due to deficiency in barium sites in undoped barium cerate (BC) composition and subsequently holes are created which follows Eqs. (3) and (4) respectively. In doped barium cerate compositions the oxygen ion vacancies are created due to substitution of higher valance Ce (4+) with lower valance Tb (3+) which is expressed in Eq. (5) [27–29].

$$\mathrm{Ba}_{Ba}^{X} = \mathrm{V}_{Ba}^{''} + \mathrm{V}_{O}^{\bullet\bullet} \tag{3}$$

$$\tfrac{1}{2}\mathrm{O}_2(\mathrm{g}) + \mathrm{V}_{O}^{\bullet\bullet} \leftrightarrow \mathrm{O}_{O}^{X} + 2h^{\bullet} \tag{4}$$

$$2Ce_{Ce}^{X} + \mathrm{Tb}_2\mathrm{O}_3 + \mathrm{O}_{O}^{X} = 2\mathrm{Tb}_{\mathrm{Ce}}^{'} + \mathrm{V}_{O}^{\bullet\bullet} + 2\mathrm{CeO}_2 \tag{5}$$

Therefore, in undoped barium cerate (BC) the majority charge carriers are holes which lead to *p*-type conductivity in the material [30]. With addition of dopant (Tb), the oxygen ion vacancies are generated in the material Eq. (5). This vacancy concentration increases with further addition of Tb in barium cerate material. In BCT1, the total electrical conductivity is lower compared to BC up to 800 °C temperature (Fig. 4a). This may be due to the reason that up to 5% of Tb doping in $Ba_{0.8}CeO_3$, the majority charge carriers (holes) move in the counter flow direction of the minority charge carriers (oxygen ions); thus reducing the overall conductivity. But above 800 °C temperature, the oxygen ion conductivity increases with increasing temperature while hole conductivity decreases [31]. In BCT2 and BCT3, the total conductivity increases with increasing temperature throughout the temperature range (Fig. 4a). This is because of oxygen ion vacancy which has become the majority charge carrier with increase in Tb concentration. In air atmosphere at elevated temperature the grain boundary conductivity is predominating in BC and BCT1 but in BCT2 and BCT3 the grain conductivity is dominating (Table 3). This may be because of the defect sites/moving charged species in lattice structure. In BC and BCT1, it is assumed that the holes are the predominant charged species that moves towards grain boundary even at slightly higher temperature and segregated along the grain boundary because of local variation in electrostatic potential and decreased density at the boundary [32]. This leads to grain boundary conductivity. But in BCT2 and BCT3, it may be the oxygen ion vacancies, the majority of which are being

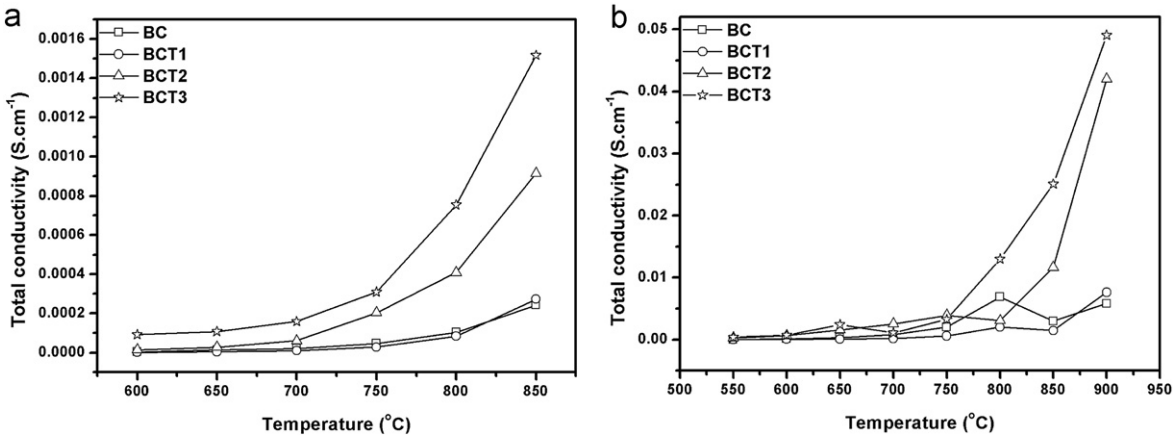

Fig. 4. Temperature dependence of total electrical conductivity of $Ba_{0.8}CeO_{3-\delta'}$ and Tb-doped $Ba_{0.8}CeO_{3-\delta'}$ materials in (a) air atmosphere and (b) moist reducing atmosphere.

Table 3
Bulk and grain boundary conductivity of undoped and Tb-doped $Ba_{0.8}CeO_{3-\delta'}$. The electrical conductivity is measured at 850 °C in air.

Sample identification code	σ_{850} (S cm^{-1})	
	Bulk/grain	Grain boundary
BC	115.454×10^{-6}	127.321×10^{-6}
BCT3	71.168×10^{-6}	202.083×10^{-6}
BCT2	602.749×10^{-6}	312.801×10^{-6}
BCT1	976.281×10^{-6}	541.498×10^{-6}

generated inside the grain because of its regular lattice structure and start moving slowly towards grain boundary [33]. Therefore, in BCT2 and BCT3 the grain conductivity is higher than grain boundary. The maximum total conductivity obtained in air atmosphere is 0.0015 S cm^{-1} at 850 °C in BCT3.

In moist reducing atmosphere, the major conducting species are OH^- and the predominant defect sites are $OH_O^{\bullet}$. The conversion of oxygen ion vacancy to protonic vacancy is shown in Eq. (2). Along with the $OH_O^{\bullet}$, the other charged species are oxide ion vacancies and holes [28]. The conversion of oxide ion vacancy to protonic vacancy depends on the gas atmosphere, partial pressure of moisture, the temperature and the corresponding dwelling time. The mechanism through which the protons move from one side of the dense material to other side is expressed using following Eqs. [34]:

$$H_2O \leftrightarrow H^+ + OH^- \quad (6)$$

$$OH^- + V_O^{\bullet\bullet} \rightarrow + OH_O^{\bullet} \quad (7)$$

$$H^+ + O^{2-} \rightarrow OH^- \quad (8)$$

$$OH^- + V_O^{\bullet\bullet} \rightarrow OH_O^{\bullet} \quad (9)$$

$$OH_O^{\bullet} \rightarrow OH^- + V_O^{\bullet\bullet} \quad (10)$$

$$OH^- \rightarrow H^+ + O^{2-} \quad (11)$$

The majority of protons move across the material through Grotthus mechanism [7]. In this mechanism the $OH_0^{\bullet}$ moves across the material through $V_0^{\bullet\bullet}$ sites by the polaron hopping process.

It is reported that the electrical conductivity of the material increases significantly in moist reducing atmosphere [5,35]. This is primarily due to factors such as nature of the moving charged species, charge carrier concentration and their mobility. The direction of the movement of charged species, concentration of defect sites and the conduction mechanism also has a significant effect to the overall conductivity of the material. In this atmosphere, protonic vacancy Eq. (2) and protons are generated by equilibrium of H_2 and water vapour with positive holes and oxide ion vacancies Eqs. (12)–(14) resulting increase in electrical conductivity [36,37].

$$H_2O + 2h^{\bullet} = 2H_i + \tfrac{1}{2}O_2 \quad (12)$$

$$H_2O + V_O^{\bullet\bullet} = 2H_i + O_O^X \quad (13)$$

$$H_2 + 2h^{\bullet} = 2H_i \quad (14)$$

It has been observed that in moist reducing atmosphere the total conductivity is increasing with increasing temperature for all the four compositions as in air atmosphere (Fig. 4b). The maximum electrical conductivity obtained in such environment is 0.049 S cm^{-1} at 900 °C for BCT3. It is observed that there appears only one semicircle when specimens are subjected to moist reducing atmosphere at higher temperature. These semicircles (in majority cases) are mainly due to grain boundary contribution to electrical conductivity (Fig. 5) [21]. Thus the grain conductivity is not that significant at higher temperature in moist reducing atmosphere. The total conductivity decreases at the temperature where first single semicircle is appearing. This is because of the fact that there is no grain contribution to total conductivity at this temperature [21,38]. Above this temperature the grain boundary is the majority conduction path for charged species. The total electrical conductivity (mainly due to grain boundary contribution) starts increasing again with temperature because of increasing oxygen ion vacancies.

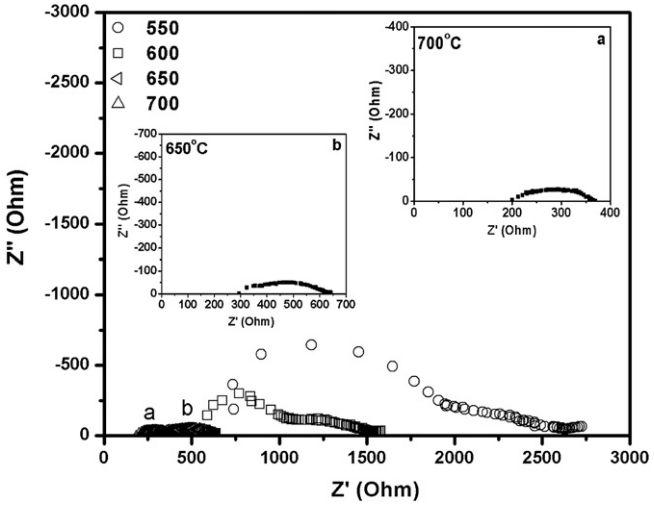

Fig. 5. Temperature dependent impedance spectra of $Ba_{0.8}Ce_{0.85}Tb_{0.15}O_{3-\delta''''}$. Insets show the extended views of spectra as shown in a and b in the figure.

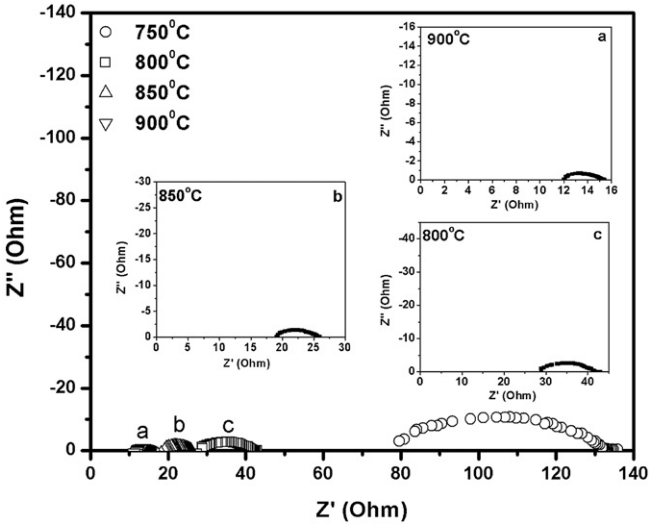

Fig. 6. Impedance spectra of $Ba_{0.8}Ce_{0.85}Tb_{0.15}O_{3-\delta''''}$ at 750, 800, 850 and 900 °C. Insets show the extended views of spectra as shown in a, b and c in the figure.

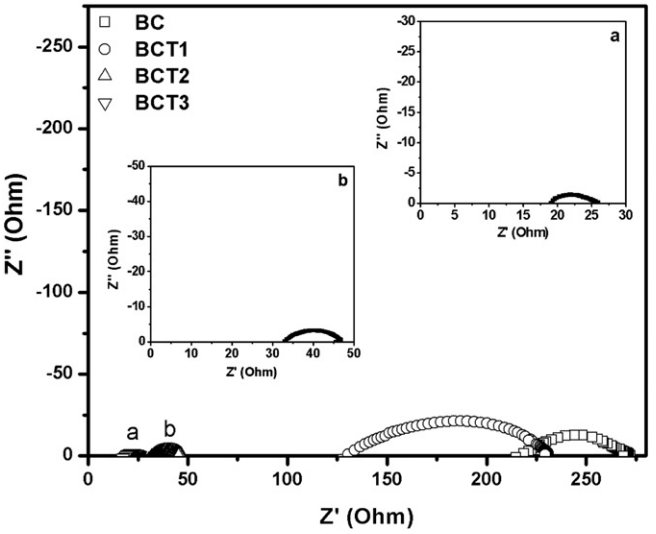

Fig. 7. Impedance spectra of $Ba_{0.8}CeO_{3-\delta'}$ and Tb-doped $Ba_{0.8}CeO_{3-\delta'}$ at 850 °C. Insets are impedance spectra for (a) BCT3 and (b) BCT2.

The unavoidable impedances [21] related to the measurement parameters and electrical contacts in sample configuration affects the impedance spectra towards higher frequency region ($>10^5$ Hz) at temperature > 700 °C. The semicircles in impedance spectra of Naquist plot are shifting towards origin for all most all the compositions both in air and moist mixture gas atmosphere with increasing operating temperature and also with increasing Tb concentration (Figs. 6 and 7). These unavoidable impedances decrease as the conductivity becomes significant at higher temperature. This shifting of semicircles towards the origin with temperature and Tb concentration may be because of the increasing conductivity in all the compositions both in air and moist reducing atmosphere.

The defect sites through which the charged species moves along the structure are different depending upon the atmosphere and temperature range [27]. In air atmosphere the holes ($h^{\cdot}$) and the oxide ion vacancies ($V_{\dot{O}}^{\cdot}$) are generally considered to be the primary defect sites whereas in moist reducing atmosphere the defect sites are holes ($h^{\cdot}$), oxide ion vacancies ($V_{\dot{O}}^{\cdot}$), proton vacancies ($OH_{\dot{O}}$) and protons ($H^{\cdot}$) [21,27]. However, all the charged species do not move in the same direction which depends mostly on the nature of the moving species. Thus O^{2-}/ OH^{-} ion and $h^{\cdot}$ / $H^{\cdot}$ move in counter flow direction while $h^{\cdot}$ and $H^{\cdot}$ move in the co-flow direction. Furthermore, the contributions of these charged species to electrical conductivity at different temperature ranges are not equal. This complex mechanism of conductivity is also evident from the temperature dependent conductivity plot where the electrical conductivity is not showing linear behaviour with temperature (Figs. 8a and b) [29].

4. Conclusions

Both undoped and Tb-doped $Ba_{0.8}CeO_{3-\delta}$ shows mixed ionic and electronic conductivity. It is observed that the contribution to electrical conductivity of different charged species as well as defect sites depends primarily on temperature and surrounding atmosphere. The electrical conductivity increases with increasing Tb concentration both in air and moist mixture gas atmosphere and also with measurement temperature. However, the conductivity in moist mixture gas atmosphere is significantly higher than that of in air atmosphere at a constant temperature. The defect sites through which the ions/conducting charged species move segregate themselves in grain boundary area rather than grain at higher temperature. Grain boundary conductivity is predominant over grain conductivity at elevated temperature in moist reducing atmosphere depending upon the composition. The maximum electrical

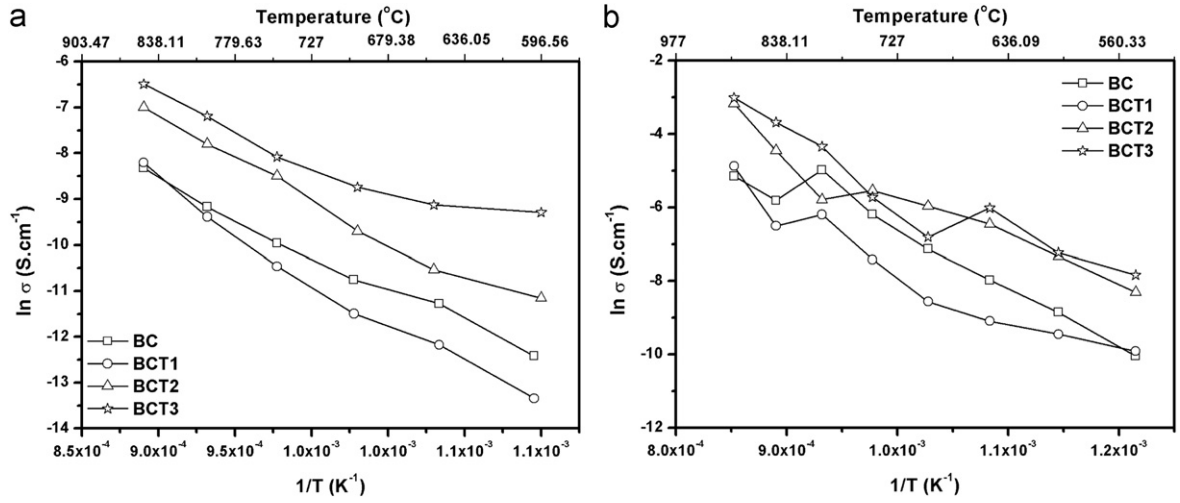

Fig. 8. Temperature dependence of electrical conductivity of $Ba_{0.8}CeO_{3-\delta'}$ and Tb-doped $Ba_{0.8}CeO_{3-\delta'}$ materials in (a) air and (b) moist reducing atmosphere.

conductivity obtained under moist reducing atmosphere is 0.049 S cm^{-1} at 900 °C for $Ba_{0.8}Ce_{0.85}Tb_{0.15}O_{3-\delta}$.

Acknowledgement

This work is financially supported by Supra Institutional Project (SIP 0023), CSIR-CGCRI, India. The authors are thankful to Director, CGCRI for his kind permission to publish this work.

References

[1] J.W. Phair, S.P.S. Badwal, Review of proton conductors for hydrogen separation, Ionics 12 (2006) 103.
[2] R. Reijers, W. Haije, Report no. ECN-E-08-091, Energy Research Centre of the Netherlands, Netherlands, 2008, pp. 1–58.
[3] X. Tan, J. Song, X. Meng, B. Meng, Preparation and characterization of $BaCe_{0.95}Tb_{0.05}O_{3-\alpha}$ hollow fibre membranes for hydrogen permeation, Journal of European Ceramic Society 32 (2012) 2351.
[4] F. Zhao, Q. Liu, S.W. Wang, K. Brinkman, F.L. Chen, Synthesis and characterization of $BaIn_{0.3-x}Y_xCe_{0.7}O_{3-\delta}$ ($x=0$, 0.1, 0.2, 0.3) proton conductors, International Journal of Hydrogen Energy 35 (2010) 4258.
[5] B. Simona, M. Battagliarin, T. Cavallin, L. Doubova, M. Fabrizio, C. Mortalo, S. Boldrini, L. Malavasic, R. Gerbasi, Journal of Materials Chemistry 18 (2008) 5120.
[6] H. Iwahara, T. Kobayashi, et al., Stability of $SrZr_{0.9}Yb_{0.1}O_{3-\delta}$ protonic conductor in atmosphere containing nitrogen oxides (NO_x), Journal of Materials Science 35 (2000) 5238.
[7] E.C.C.D. Souza, R. Muccillo, Properties and applications of perovskite proton conductors, Materials Research 13 (3) (2010) 385.
[8] H. Iwahara, Proton conducting ceramics and their applications, Solid State Ionics 86–88 (1996) 9.
[9] A. Subramaniyan, J. Tong, R.P. O'Hayre, N.M. Sammes, Sintering studies on 20 mol% yttrium-doped barium cerate, Journal of American Ceramic Society 94 (6) (2011) 1800.
[10] A. Suresh, J. Basu, C.B. Carter, N. Sammes, B.A. Wilhite, Synthesis of cobalt-doped barium cerate-zirconate and its evaluation for hydrogen production and electrochemical characterization, Journal of Materials Science 45 (2010) 3215.
[11] J. Liu, Y. Li, et al., Proton conduction at intermediate temperature and its application in ammonia synthesis at atmospheric pressure of $BaCe_{1-x}Ca_xO_{3-\alpha}$, Journal of Materials Science 45 (2010) 5860.
[12] L. Yang, S.Z. Wang, X.O. Lou, M.L. Liu, Electrical conductivity and electrochemical performance of cobalt-doped $BaZr_{0.1}Ce_{0.7}Y_{0.2}O_{3-\delta}$ cathode, International Journal of Hydrogen Energy 36 (2011) 2266.
[13] N.V. Sharova, V.P. Gorelov, Electroconductivity and ion transport in protonic solid electrolytes $BaCe_{0.85}R_{0.15}O_{3-\delta}$, Russian Journal of Electrochemistry 39 (5) (2003) 461.
[14] H. Taherparvara, J.A. Kilnera, R.T. Bakerb, M. Sahibzada, Effect of humidification at anode and cathode in proton-conducting SOFCs, Solid State Ionics 162–163 (2003) 297.
[15] H.J. Park, C. Kwak, K.H. Lee, S.M. Lee, E.S. Lee, Interfacial protonic conduction in ceramics, Journal of European Ceramic Society 29 (2009) 2429.
[16] R.D. Carneim, T.M. Besmann, T.R. Armstrong, Metals and Ceramics Division, Report no. TN 37831, Oak Ridge National Laboratory, Oke Ridge, USA, 2001.
[17] Y. Yamazaki, R.H. Sanchez, S.M. Haile, Cation non-stoichiometry in yttrium-doped barium zirconate: phase behaviour, microstructure, and proton conductivity, Journal of Materials Chemistry 20 (2010) 8158.
[18] J.D. Wang, Y.H. Xie, Z.F. Zhang, R.Q. Liu, Z.J. Lee, Protonic conduction in Ca^{2+}-doped $La_2M_2O_7$ (M=Ce, Zr) with its application to ammonia synthesis electrochemically, Materials Research Bulletin 40 (2005) 1294.
[19] D. Dionysioua, X.W. Qia, Y.S. Lina, G. Mengb, D. Peng, Preparation and characterization of proton conducting terbium doped strontium cerate membranes, Journal of Membrane Science 154 (1999) 143.
[20] P. Pasierb, J. Wyrwa, M. Rekas, Electrical properties of acceptor-doped $BaCeO_3$, Ceram Materials 62 (3) (2010) 311.
[21] S.D. Flint, R.C.T. Slade, Investigation of radiation-grafted PVDF-g-polystyrene-sulfonic-acid ion exchange membranes for use in hydrogen oxygen fuel cells, Solid State Ionics 97 (1997) 457.
[22] D. Shima, S.M. Haile, The influence of cation non-stoichiometry on the properties of undoped and gadolinia-doped barium cerate, Solid State Ionics 97 (1997) 443.
[23] Q.L. Gan, M.G. Lin, Mixed conduction in Tb_2O_3 doped $BaCeO_3$, Chinese Journal of Chemistry 24 (2006) 1564.
[24] K.E.J. Eurenius, Ph.D. Thesis, University of Gothenburg, Gothenburg, Sweden, ISBN: 978-91-628-7897-9, 2009.
[25] J.W. Phair, S.P.S. Badwal, Materials separation membrane in hydrogen and oxygen production and future power generation, Science and Technology of Advanced Materials 7 (2006) 792.

[26] K.G. Kasic, A.M. Gryn, T. Lendze, S. Molin, B. Kusz, M. Gazda, Synthesis of acceptor-doped Ba–Ce–Zr–O perovskites, Crystal Research Technology 45 (2010) 1251.
[27] E. Gorbova, V. Maragou, D. Medvedev, A. Demin, P. Tsiakaras, Investigation of the protonic conduction in Sm doped $BaCeO_3$, Journal of Power Sources 181 (2008) 207.
[28] S.M. Haile, G. Stanefe, K.H. Ryu, Non-stoichiometry, grain boundary transport and chemical stability of proton conducting perovskites, Journal of Materials Science 36 (2001) 1149.
[29] J.M.J. Luo, K.T. Chuang, A.R. Sanger, Stability and electric conductivity of barium cerate perovskites Co-doped with praseodymium, The Open Fuels & Energy Science Journal 1 (2008) 7.
[30] F.L. Chen, O.T. Sørensen, G.Y. Meng, D.K. Peng, Preparation of Nd-doped $BaCeO_3$ proton-conducting ceramic and its electrical properties in different atmospheres, Journal of the European Ceramic Society 18 (1998) 1389.
[31] A. Radojković, M. Žunić, S.M. Savić, G. Branković, Z. Branković, Chemical stability and electrical properties of Nd doped $BaCe_{0.9}Y_{0.1}O_{3-\delta}$ as a high temperature proton conducting electrolyte for IT-SOFC, Ceramics International 39 (1) (2013) 307–313.
[32] K.P. McKenna, A.L. Shluger, First-principle calculations of defects near a grain boundary in MgO, Physical Review B 79 (2009) 224116.
[33] K.C. Yoo, S.M. Johnson, W.F. Regnault, Lattice defects within grain volumes that affect the electrical quality of cast polycrystalline silicon solar-cell materials, Journal of Applied Physics 57 (6) (1985) 2258.
[34] S. Nag, S. Mukhopadhyay, R.N. Basu, Development of mixed conducting dense nickel/ Ca-doped lanthanum zirconate cermet for gas separation application, Materials Research Bulletin 47 (3) (2012) 925.
[35] H. Jena, K.V.G. Kutty, T.R.N. Kutty, Proton transport and structural relations in hydroxyl-bearing BaTiO3 and its doped compositions synthesised by wet-chemical methods, Materials Research Bulletin 39 (2004) 489.
[36] H. Matsumoto, T. Shimura, T. Higuchi, H. Tanaka, et al., Protonic–electronic mixed conduction and hydrogen permeation in $BaCe_{0.9-x}Y_{0.1}Ru_xO_{3-\alpha}$, Journal of the Electrochemical Society 152 (3) (2005) A488.
[37] G. Ma, T.S. Shimura, H. Iwahara, Ionic conduction and nonstoichiometry in $Ba_xCe_{0.90}Y_{0.10}O_{3-\alpha}$, Solid State Ionics 110 (1998) 103.
[38] F.M.M. Snijkers, A. Buekenhoudt, J.J. Luyten, J. Cooymans, M. Mertens, Proton conductivity in perovskite type yttrium doped barium hafnate, Scripta Materialia 51 (2004) 1129.